




## Article

# Human Hepatocyte 4-Acetoxy-*N,N*-Diisopropyltryptamine Metabolite Profiling by Reversed-Phase Liquid Chromatography Coupled with High-Resolution Tandem Mass Spectrometry

Sara Malaca <sup>1</sup>, Marilyn A. Huestis <sup>2</sup> , Leonardo Lattanzio <sup>3</sup>, Luigi T. Marsella <sup>3</sup>, Adriano Tagliabracci <sup>1</sup> , Jeremy Carlier <sup>1,\*</sup>  and Francesco P. Busardò <sup>1</sup>

<sup>1</sup> Unit of Forensic Toxicology, Section of Legal Medicine, Department of Excellence of Biomedical Sciences and Public Health, Marche Polytechnic University, Via Tronto 10/a, 60126 Ancona, Italy; smalaca@hotmail.com (S.M.); a.tagliabracci@staff.univpm.it (A.T.); fra.busardo@libero.it (F.P.B.)

<sup>2</sup> Institute of Emerging Health Professions, Thomas Jefferson University, Philadelphia, PA 19107, USA; marilyn.huestis@gmail.com

<sup>3</sup> Forensic Medicine, Department of Biomedicine and Prevention, University of Rome Tor Vergata, 00133 Rome, Italy; leonardolattanzio1@gmail.com (L.L.); marsella.luigi@gmail.com (L.T.M.)

\* Correspondence: jerem.carlier@gmail.com; Tel.: +39-071-220-6212



**Citation:** Malaca, S.; Huestis, M.A.; Lattanzio, L.; Marsella, L.T.; Tagliabracci, A.; Carlier, J.; Busardò, F.P. Human Hepatocyte 4-Acetoxy-*N,N*-Diisopropyltryptamine Metabolite Profiling by Reversed-Phase Liquid Chromatography Coupled with High-Resolution Tandem Mass Spectrometry. *Metabolites* **2022**, *12*, 705. <https://doi.org/10.3390/metabo12080705>

Academic Editors: Markus R. Meyer and Lea Wagmann

Received: 1 July 2022

Accepted: 26 July 2022

Published: 29 July 2022

**Publisher's Note:** MDPI stays neutral with regard to jurisdictional claims in published maps and institutional affiliations.



**Copyright:** © 2022 by the authors. Licensee MDPI, Basel, Switzerland. This article is an open access article distributed under the terms and conditions of the Creative Commons Attribution (CC BY) license (<https://creativecommons.org/licenses/by/4.0/>).

**Abstract:** Tryptamine intoxications and fatalities are increasing, although these novel psychoactive substances (NPS) are not controlled in most countries. There are few data on the metabolic pathways and enzymes involved in tryptamine biotransformation. 4-acetoxy-*N,N*-diisopropyltryptamine (4-AcO-DiPT) is a synthetic tryptamine related to 4-hydroxy-*N,N*-diisopropyltryptamine (4-OH-DiPT), 4-acetyloxy-*N,N*-dipropyltryptamine (4-AcO-DPT), and 4-acetoxy-*N,N*-dimethyltryptamine (4-AcO-DMT). The aim of this study was to determine the best 4-AcO-DiPT metabolites to identify 4-AcO-DiPT consumption through human hepatocyte metabolism and high-resolution mass spectrometry. 4-AcO-DiPT metabolites were predicted *in silico* with GLORYx freeware to assist in metabolite identification. 4-AcO-DiPT was incubated with 10-donor-pooled human hepatocytes and sample analysis was performed with reversed-phase liquid chromatography coupled with high-resolution tandem mass spectrometry (LC-HRMS/MS) in positive- and negative-ion modes. Software-assisted LC-HRMS/MS raw data mining was performed. A total of 47 phase I and II metabolites were predicted, and six metabolites were identified after 3 h incubation following ester hydrolysis, *O*-glucuronidation, *O*-sulfation, *N*-oxidation, and *N*-dealkylation. All second-generation metabolites were derived from the only first-generation metabolite detected after ester hydrolysis (4-OH-DiPT). The metabolite with the second-most-intense signal was 4-OH-iPT-sulfate followed by 4-OH-DiPT-glucuronide, indicating that glucuronidation and sulfation are common in this tryptamine's metabolic pathway. 4-OH-DiPT, 4-OH-iPT, and 4-OH-DiPT-*N*-oxide are suggested as optimal biomarkers to identify 4-AcO-DiPT consumption.

**Keywords:** tryptamine; 4-AcO-DiPT; *in silico* prediction; hepatocyte metabolism; liquid chromatography-high-resolution tandem mass spectrometry (LC-HRMS/MS); data mining

## 1. Introduction

Tryptamines are a class of new psychoactive substances (NPS) that share a core structure with the neurotransmitter serotonin, or 5-hydroxytryptamine (5-HT). Tryptamine's psychedelic effects are produced through agonism of the 5-HT<sub>2A</sub> and 5-HT<sub>2C</sub> receptors, with additional contribution from other monoamine transporters [1–10]. Diverse tryptamine structures have different receptor affinities and resultant effects. 4-AcO-DiPT is a synthetic tryptamine related to 4-hydroxy-*N,N*-diisopropyltryptamine (4-OH-DiPT), 4-acetyloxy-*N,N*-dipropyltryptamine (4-AcO-DPT), and 4-acetoxy-*N,N*-dimethyltryptamine (4-AcO-

DMT), which currently are not controlled in many countries. 4-AcO-DiPT was identified as early as July 2004, with charges against vendors selling the drug to the public; however, there were no convictions and there was no determination of the legal status of 4-AcO-DiPT [11]. Although the current use of psychedelics is low, tryptamine intake is increasing [1,10] despite limited data on prevalence and patterns of intake. According to psychonauts' experiences, as reported on the Erowid website, 4-AcO-DiPT is available online and typically administered orally, with effects similar to those of hallucinogenic mushrooms and 2-(4-bromo-2,5-dimethoxyphenyl)-ethanamine (2C-B) [12]. 4-AcO-DiPT is a white powder available in freebase and HCl salt forms. Both are orally active, with the lower molecular weight freebase being about 10% more potent than the same weight of the HCl salt. 4-AcO-DiPT and 4-OH-DiPT have similar effects if taken orally, though dosage might be different. Oral 4-AcO-DiPT doses start at 3–5 mg; 5–15 mg is considered a "light" dose, while higher doses range between 25 and 40 mg. Users self-report 15–30 mg doses, with onset of effects in 20–60 min, depending on dosage form and stomach contents, and duration of 2–4 h. Its effects, which can appear within 1–4 h, are dose-dependent and include hallucination, dissociation, confusion, and flashbacks, as reported on Erowid by a 4-AcO-DiPT user [12]. Over the last decade, there were few intoxication cases and even fewer fatalities due to tryptamines reported in the European Union and North America, although this is likely an underestimation due to missed detections. There are few data on metabolic pathways and specific enzymes involved in tryptamine biotransformation, but it appears that there is not a common metabolic pathway, with the nature and position of substituents changing metabolism. Overall, psychedelic tryptamine use is increasing, raising the importance of laboratory identification of specific metabolites to verify intake and identify potential public health NPS outbreaks. The aim of this study was to determine the optimal 4-AcO-DiPT metabolite biomarkers of consumption for clinical and forensic applications, using *in silico* metabolite prediction, human hepatocyte metabolism, LC-HRMS/MS analysis, and software-assisted data mining.

## 2. Results

### 2.1. *In Silico* Metabolite Predictions

*In silico* metabolite predictions are reported in Supplementary Table S1. A total of 47 phase I and II metabolites were predicted, with 10 first-generation metabolites (pM 1–pM 10, by decreasing score) and 37 s-generation metabolites (pM X.1, pM X.4, by decreasing score, and pMX indicating the corresponding first-generation metabolite) (Table 1). First-generation metabolites included hydroxylation, deisopropylation, carboxylation, ester hydrolysis, glucuronidation, and deamination. Second-generation metabolites involved phase I (hydroxylation, dealkylation, carboxylation, and deisopropylation) and phase II (glucuronidation and sulfation) reactions. All predicted metabolites were incorporated in a ddMS<sup>2</sup> inclusion list to support LC-HRMS/MS analyses (Supplementary Table S1), and all predicted metabolic transformations were incorporated in the list of potential reactions to support automatic data mining.

### 2.2. 4-AcO-DiPT Fragmentation Pattern

The 4-AcO-DiPT fragmentation pattern is shown in Figure 1. In positive-ionization mode, ions with  $m/z$  202.0866 resulted from a loss of the diisopropyl amine group followed by loss of the acetyl group producing ions with  $m/z$  160.0758, the fragment with the most intense signal. Further fragmentation yielded ions with  $m/z$  132.0808 then 115.0539 through carbon monoxide and ammonia losses, respectively. Ion  $m/z$  117.0573 was a radical cation typically yielded from hydroxyindole alkylamines [13].  $\alpha$ - and  $\beta$ -cleavage at the nitrogen of the ethylamine chain yielded fragments with  $m/z$  114.1275 and 102.1278, respectively. Fragments with  $m/z$  72.0805 were further produced by isopropyl loss from ions with  $m/z$  114.1275. In addition, the fragments with  $m/z$  259.1815 in negative ionization mode indicate an acetyl loss on the parent drug.

**Table 1.** Molecular structure, elemental composition, metabolic transformation, and predictive score of in silico-predicted 4-AcO-DiPT metabolites.

Predicted Metabolite (pM)	Transformation	Elemental Composition	Score (%)
pM1	N-Hydroxylation	C <sub>18</sub> H <sub>27</sub> N <sub>2</sub> O <sub>3</sub>	63
pM1.1	O-Glucuronidation	C <sub>25</sub> H <sub>30</sub> N <sub>2</sub> O <sub>8</sub>	30
pM1.2	N-Deisopropylation	C <sub>16</sub> H <sub>21</sub> NO <sub>3</sub>	22
pM1.3	Hydroxylation	C <sub>19</sub> H <sub>28</sub> NO <sub>4</sub>	22
pM1.4	Hydroxylation (C1'')	C <sub>18</sub> H <sub>26</sub> N <sub>2</sub> O <sub>4</sub>	21
pM2	Hydroxylation (C2'')	C <sub>18</sub> H <sub>26</sub> N <sub>2</sub> O <sub>3</sub>	63
pM2.1	O-Sulfation	C <sub>18</sub> H <sub>24</sub> N <sub>3</sub> O <sub>7</sub> S	60
pM2.2	O-Glucuronidation	C <sub>24</sub> H <sub>32</sub> N <sub>2</sub> O <sub>10</sub>	39
pM2.3	Dealkylation	C <sub>17</sub> H <sub>24</sub> N <sub>2</sub> O <sub>2</sub>	21
pM2.4	Hydroxylation (C11)	C <sub>19</sub> H <sub>26</sub> N <sub>2</sub> O <sub>4</sub>	21
pM2.5	Carboxylation (C9)	C <sub>19</sub> H <sub>24</sub> N <sub>2</sub> O <sub>5</sub>	21
pM3	Deisopropylation	C <sub>15</sub> H <sub>20</sub> N <sub>2</sub> O <sub>2</sub>	63
pM3.1	Hydroxylation (C1'')	C <sub>16</sub> H <sub>20</sub> N <sub>2</sub> O <sub>3</sub>	35
pM3.2	Depropylation	C <sub>13</sub> H <sub>14</sub> O <sub>3</sub>	35
pM3.3	N-Hydroxylation	C <sub>15</sub> H <sub>20</sub> N <sub>2</sub> O <sub>3</sub>	35
pM3.4	N-Deisopropylation	C <sub>12</sub> H <sub>14</sub> N <sub>2</sub> O <sub>2</sub>	35
pM4	Hydroxylation (acetyl)	C <sub>18</sub> H <sub>26</sub> N <sub>2</sub> O <sub>3</sub>	34
pM4.1	O-Glucuronidation	C <sub>23</sub> H <sub>32</sub> N <sub>2</sub> O <sub>9</sub>	28
pM4.2	O-Sulfation	C <sub>17</sub> H <sub>24</sub> N <sub>2</sub> O <sub>6</sub> S	24
pM5	Carboxylation (acetyl)	C <sub>19</sub> H <sub>26</sub> N <sub>2</sub> O <sub>3</sub>	34
pM5.1	O-Glucuronidation	C <sub>26</sub> H <sub>36</sub> N <sub>2</sub> O <sub>9</sub>	31
pM5.2	N-Hydroxylation	C <sub>18</sub> H <sub>25</sub> N <sub>2</sub> O <sub>5</sub>	20
pM5.3	Deisopropylation	C <sub>15</sub> H <sub>18</sub> N <sub>2</sub> O <sub>4</sub>	20
pM5.4	Hydroxylation (C1'')	C <sub>18</sub> H <sub>24</sub> N <sub>2</sub> O <sub>5</sub>	20
pM6	Ester hydrolysis	C <sub>19</sub> H <sub>26</sub> N <sub>2</sub> O	34
pM6.1	O-Sulfation	C <sub>16</sub> H <sub>24</sub> N <sub>2</sub> O <sub>4</sub> S	32
pM6.2	O-Glucuronidation	C <sub>22</sub> H <sub>32</sub> N <sub>2</sub> O <sub>7</sub>	29
pM6.3	Hydroxylation (C1'')	C <sub>16</sub> H <sub>24</sub> N <sub>2</sub> O <sub>2</sub>	20
pM6.4	N-Hydroxylation	C <sub>16</sub> H <sub>25</sub> N <sub>2</sub> O <sub>2</sub>	20
pM7	Hydroxylation (C2)	C <sub>16</sub> H <sub>24</sub> N <sub>2</sub> O <sub>2</sub>	25
pM8	N-Glucuronidation	C <sub>12</sub> H <sub>13</sub> NO <sub>3</sub>	20
pM9	Deamination (to aldehyde)	C <sub>12</sub> H <sub>13</sub> NO <sub>3</sub>	20
pM10	Deamination (to alcohol)	C <sub>12</sub> H <sub>11</sub> NO <sub>3</sub>	20

### 2.3. Metabolite Identification

LC-HRMS data were automatically processed to produce a list of six potential metabolites that were manually checked by the operators. The 4-AcO-DiPT LC-HRMS peak area was  $3.00 \times 10^7$  in the 3 h incubation with hepatocytes, i.e., 375 times lower than that of the 0 h incubation ( $1.12 \times 10^{10}$ ). Six metabolites were identified after 3 h incubation following ester hydrolysis, O-glucuronidation, O-sulfation, N-oxidation, and N-dealkylation. All second-generation metabolites were derived from the only first-generation metabolite detected, which was produced by ester hydrolysis (4-OH-DiPT, M4). The metabolites are listed from M1 to M6 by ascending retention time (Table 2). The five remaining metabolites all derived from M4 with further phase I and II transformations, including N-deisopropylation (4-OH-iPT, M1 and 4-OH-iPT-sulfate, M2) and N-oxidation at the ethylamine chain (4-OH-DiPT-N-oxide, M6), and O-sulfation (M2 and 4-OH-DiPT-sulfate, M5) and O-glucuronidation (4-OH-DiPT-glucuronidate, M3) in the indole ring. The fragmentation pattern of 4-AcO-DiPT metabolites is shown in Figure 1. The metabolic pathway of the major metabolites is suggested in Figure 2. An extracted-ion chromatogram of 4-AcO-DiPT

and metabolites in positive-ionization mode obtained after 3 h incubation with human hepatocytes is presented in Figure 3.

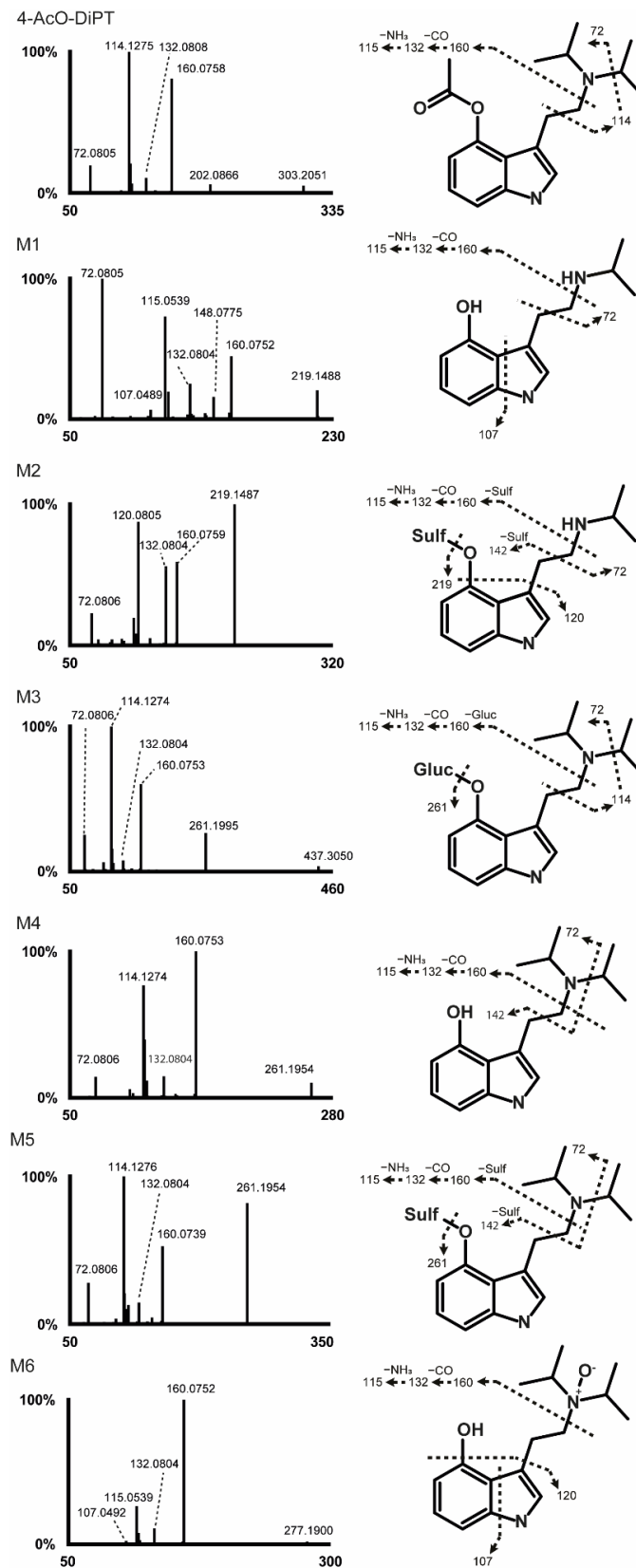


**Figure 1.** 4-AcO-DiPT high-resolution tandem-mass-spectrometry spectrum and suggested fragmentation in positive-ionization mode.

**Table 2.** Metabolic transformation, retention time (RT), accurate mass of molecular ion (hydrogen adduct in positive-ionization mode  $[M + H]^+$ ), elemental composition, deviation from theoretical accurate mass, and liquid chromatography–high-resolution mass spectrometry peak area of 4-AcO-DiPT and metabolites after 3 h incubation with human hepatocytes (HESI positive mode, HESI negative mode).

ID	Transformation	RT (min)	$[M + H]^+$	Elemental Composition	Mass Error (ppm)	Peak Areas (HESI+, HESI–)
M1	Ester hydrolysis + <i>N</i> -Deisopropylation	6.31	219.1489	$C_{13}H_{18}N_2O$	−1.21	$1.10 \times 10^8$
M2	Ester hydrolysis + <i>N</i> -Deisopropylation + <i>O</i> -Sulfation	7.24	299.1057	$C_{13}H_{18}N_2O_4S$	−1.23	$3.50 \times 10^7, 5.90 \times 10^7$
M3	Ester hydrolysis + <i>O</i> -Glucuronidation	8.30	437.2277	$C_{22}H_{32}N_2O_7$	−1.45	$2.94 \times 10^8, 2.60 \times 10^7$
M4	Ester hydrolysis	11.82	261.1955	$C_{16}H_{24}N_2O$	−2.25	$4.19 \times 10^9$
M5	Ester hydrolysis + <i>O</i> -Sulfation	12.11	341.1525	$C_{16}H_{24}N_2O_4S$	−1.42	$4.47 \times 10^7, 2.79 \times 10^7$
M6	Ester hydrolysis + <i>N</i> -Oxidation	12.53	277.1907	$C_{16}H_{24}N_2O_2$	−1.35	$7.76 \times 10^6$
Parent	no transformation	15.02	303.2059	$C_{18}H_{26}N_2O_2$	−2.67	$3.00 \times 10^7$

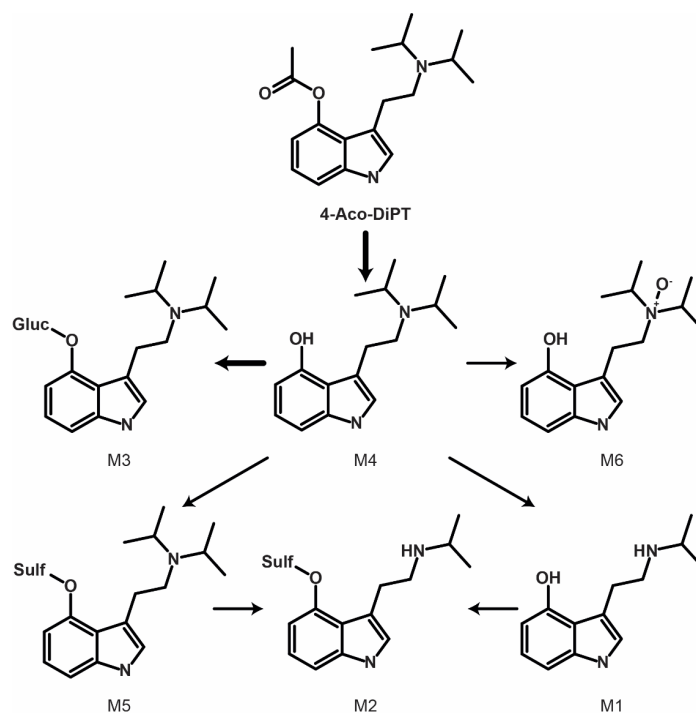


**Figure 2.** Suggested metabolic fate of 4-AcO-DiPT. Bold indicates major transformations.

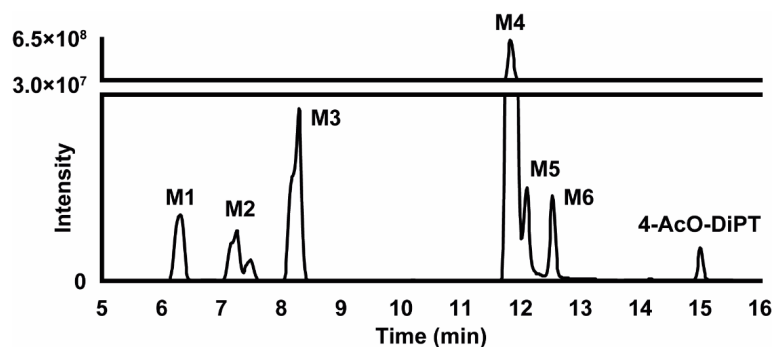


**Figure 3.** Extracted-ion chromatogram of 4-AcO-DiPT and metabolites in positive-ionization mode obtained after 3 h incubation with human hepatocytes. Mass tolerance: 5 ppm;  $m/z$  values: 219.1489, 261.1955, 277.1907, 299.1057, 303.2059, 341.1525, and 437.2277.

### 2.3.1. Phase I Metabolites

#### Ester Hydrolysis

Among the detected metabolites, M4, eluted at 11.82 min, generated the most intense signal with a base peak at  $m/z$  261.1954. 4-OH-DiPT transformation occurred with the loss of the acetyl group and with hydrolysis occurring in the hydroxyl group of the indole ring, as demonstrated by the production of fragments with  $m/z$  160.0753, 114.1274, and 117.0573. The fragments from negative-ionization mode at  $m/z$  132.0243, 114.1275, 132.0804, and 72.0806 showed that the indole core and ethylamine chains were intact. The acetyl loss is indicated by the mass shift of +42.0104 Da from the parent and a difference of -2C -2H -1O on the elemental composition.

M1, M2, M3, M5, and M6 were produced after ester hydrolysis and other metabolic reactions. M3 was detected as a double peak with the same fragmentation pattern.

#### Ester Hydrolysis and *N*-Deisopropylation

M1 eluted at 6.31 min, and was formed after *N*-deisopropylation following ester hydrolysis. A fragment with  $m/z$  160.0752 in the MS/MS spectrum clearly identifies that this reaction occurred in the isopropyl group. 4-OH-iPT revealed a mass shift of +84.0570 Da and a difference of elemental composition of -5C -8H -1O proves this metabolic reaction.

#### Ester Hydrolysis and *N*-Oxidation

M6 was detected at 12.53 min and was produced by oxidation on the indole ring after ester hydrolysis. Fragments with  $m/z$  160.0752, 107.0492, and 115.0539 showed that this transformation did not occur in the indole ring, but instead in the diisopropyl amine group of the molecule. This metabolite presented a mass shift of +26.0152 Da and a difference in elemental composition of -2C -2H. The retention time of 4-OH-DiPT-*N*-oxide was later than that of M4 (4-OH-DiPT), indicating *N*-oxidation [14–16].

### 2.3.2. Phase II Metabolites

#### Ester Hydrolysis and *O*-Glucuronidation

M3, detected at 8.20 min, had the second-most-intense signal. This metabolite was formed after ester hydrolysis and glucuronidation. 4-OH-DiPT-glucuronidate presented a mass shift of -134.0218 Da, differing by +4C +6H +5O from the elemental composition of the parent drug. The presence of fragments with  $m/z$  160.0753 and 114.1274 clearly indicates no transformation in the indole core or the ethylamine chain. Actually, the signal that was detected in negative ionization mode suggests that a glucuronidation reaction occurred.

#### Ester Hydrolysis and *O*-Sulfation

M5 eluted at 12.11 min, with fragments having  $m/z$  160.0752 and 115.0539 indicating no reaction at the indole core or the ethylamine chain. 4-OH-DiPT-sulfate showed a mass shift of -37.9466 Da and a difference of -2C -2H +2O +1S on its elemental composition.

#### Ester Hydrolysis, *N*-Deisopropylation, and *O*-Sulfation

M2, eluting at 7.24 min, resulted from ester hydrolysis, *N*-deisopropylation, and sulfation (produced by M1 *O*-sulfation). The fragments with  $m/z$  120 prove that no changes were made in the indole core. 4-OH-iPT-sulfate had a mass shift of +4.1002 Da and a difference of -5C -8H +2O +1S in its elemental composition. M2 produced fragments with  $m/z$  219.1487 by sulfate loss, and similar fragments to those of M1.

The fact that a signal was also identified in negative ionization mode suggests that a sulfation reaction occurred to generate both metabolites (M2 and M5).

## 3. Discussion

In silico metabolite predictions alone are not sufficient to identify the metabolism of specific drugs; however, compilation of HRMS/MS inclusion and exclusion lists and a list of



potential metabolic transformations is key to successful Compound Discoverer processing workflow (Supplementary Table S1) and for aiding manual metabolite identification. All six metabolites were predicted. The main phase I and II reactions occurred in the hydroxyl group of the indole ring and in the isopropyl group after ester hydrolysis.

4-AcO-DiPT was incubated with human hepatocytes, which have been proven more suitable for metabolite profiling than human liver microsomes [17]. Hepatocytes are more representative of the physiological liver environment containing both phase I and II drug-metabolizing enzymes, cofactors, and drug transporters [18]. All of these factors allow a better estimation of *in vivo* metabolism.

The M4 signal was the most intense metabolite signal detected 3 h after incubation with hepatocytes, followed by glucuronidation generating M3. Interestingly, the most intense metabolite (M4) was also detected in the control samples without hepatocytes at 0 and 3 h and at 0 h incubation with hepatocytes but at a much lower intensity than after 3 h incubation, meaning that, although M4 is formed through an enzymatic reaction, it is also spontaneously formed during incubation to a lesser extent. This indicates that M4 formation was overestimated in our experiments. When analyzing authentic samples, digestion (with  $\beta$ -glucuronidase/sulfatase) is preferred to increase the M4 signal. To further understand where the glucuronidation occurred in M3, the 3 h incubations with hepatocytes was reanalyzed after enzymatic hydrolysis with  $\beta$ -glucuronidase, suggesting which part of the molecule was glucuronidated.  $\beta$ -Glucuronidase catalyzes the hydrolysis of *O*-glucuronides and not *N*-glucuronides. Comparing the control sample (same hydrolysis conditions but without  $\beta$ -glucuronidase) to the sample with  $\beta$ -glucuronidase, M3 was not present, revealing that the reaction occurred at the hydroxyl group of the molecule and not on the amine group.

An additional consideration is that samples were resuspended in a ratio of 80:20 mobile phase (A:B) to guarantee maximum recovery of the analyte. This can explain the double peak detected for M3. Better peak shapes would be obtained if samples were resuspended with a lower percentage of acetonitrile (mobile phase B). To assure that the double peak was not an isomer, another test was made using a ratio of 95:5 mobile phase (A:B) where no double peak was detected.

Since the parent drug is most likely degraded as the acetyl group is eliminated quickly, toxicologists could report 4-OH-DiPT (M4)-positive cases as from 4-AcO-DiPT intake. The second-most-intense metabolite was M3 (4-OH-DiPT-glucuronide) followed by M1 (4-OH-iPT), indicating that glucuronidation and dealkylation are common in this tryptamine's metabolic pathway. Others propose that tryptamines do not have a common metabolic pathway and that metabolism changes depending on the nature and position of their substituents, with demethylation, hydroxylation, and dealkylation being the most common phase I reactions, followed by glucuronidation or sulfation [19–24]. 4-OH-DiPT, 4-OH-iPT, and 4-OH-DiPT-*N*-oxide are proposed as biomarkers of 4-AcO-DiPT consumption, but the rapid enzymatic hydrolysis and lower spontaneous hydrolysis of 4-AcO-DiPT to 4-OH-DiPT might create a problem in discerning 4-AcO-DiPT from 4-OH-DiPT consumption. If the parent drug is present even in low concentrations, the ingested drug would be clear, but there is no available information regarding detection of this drug in authentic samples. These results require *in vivo* confirmation, which is challenging due to the lower prevalence indicated by the small number of 4-AcO-DiPT seizures in recent years.

## 4. Materials and Methods

### 4.1. *In Silico* Metabolites Prediction

4-AcO-DiPT metabolites were predicted with the online GLORYx freeware [25,26]. The metabolite list was generated using the 4-AcO-DiPT with the “phase I and phase II metabolism” option (Table 1, 1st generation). Metabolites with a score higher than 0.40 were selected and reprocessed to simulate a second-step metabolism reaction (Table 1, 2nd generation); the second-generation metabolite score was multiplied by the

first-generation metabolite score and scores higher than 0.20 were added to the inclusion list (Supplementary Table S1).

#### 4.2. Chemicals and Reagents

4-AcO-DiPT was obtained from Cayman Chemical (Ann Arbor, MI, USA) and diclofenac was acquired from Sigma Aldrich (Milan, Italy). Stock standards of these chemicals were prepared to 1 mg/mL in LC-MS-grade methanol (Carlo Erba; Cornaredo, Italy). Standards were stored at  $-20\text{ }^{\circ}\text{C}$  until analysis. Ten-donor-pooled cryopreserved human hepatocytes, thawing medium (TM), and 0.4% trypan blue were purchased from Lonza (Basel, Switzerland). L-Glutamine, HEPES (2-[4-(2-hydroxyethyl)-1-piperazinyl]ethanesulfonic acid), and Williams' Medium E were obtained from Sigma Aldrich. L-Glutamine and HEPES were dissolved in Williams' Medium E to 2 and 20 mmol/L, respectively, prior to analysis. The supplemented Williams' Medium E (sWME) was stored at  $4\text{ }^{\circ}\text{C}$  until incubation. LC-MS-grade acetonitrile, water, and formic acid were obtained from Carlo Erba (Cornaredo, Italy).

#### 4.3. Hepatocytes Incubation

Incubations were conducted as previously described, with small adjustments [27]. Hepatocytes, thawed at  $37\text{ }^{\circ}\text{C}$ , were lightly mixed with 50 mL TM in a 50 mL polypropylene conical tube maintained at the same temperature. The tube was centrifuged at  $100\times g$  for 5 min and the pellet washed with 50 mL sWME at  $37\text{ }^{\circ}\text{C}$ . After centrifugation under the same conditions, cells were resuspended in 2 mL sWME. Hepatocyte viability was evaluated with the trypan blue exclusion test, and sWME volume adjusted to  $2 \times 10^6$  viable cells/mL. Incubations were prepared in sterile 24-well culture plates with 250  $\mu\text{L}$  hepatocyte suspension and 250  $\mu\text{L}$  4-AcO-DiPT at 20  $\mu\text{mol/L}$  in sWME at  $37\text{ }^{\circ}\text{C}$ . Metabolic reactions were then interrupted with 500  $\mu\text{L}$  ice-cold acetonitrile. Negative controls, i.e., hepatocytes in sWME without 4-AcO-DiPT and 4-AcO-DiPT in sWME without hepatocytes, were incubated for 3 h under the same conditions. Diclofenac was also incubated under the same conditions to ensure proper metabolic activity.

#### 4.4. Sample Preparation

For sample preparation, 100  $\mu\text{L}$  hepatocyte supernate was vortexed with 100  $\mu\text{L}$  acetonitrile, centrifuged at  $15,000\times g$  for 10 min at room temperature, and the supernates were dried under nitrogen at  $37\text{ }^{\circ}\text{C}$ . Residues were reconstituted with 150  $\mu\text{L}$  mobile phase A (MPA): mobile phase B (MPB) (8:2 *v/v*), mixed well, and centrifuged for 10 min at  $15,000\times g$  at room temperature, and the supernates were transferred into glass inserts in LC autosampler vials. The sample injection volume was 15  $\mu\text{L}$ .

#### 4.5. Instrumental Conditions

LC-HRMS/MS analyses were performed on a DIONEX UltiMate 3000 liquid chromatograph coupled with a Q-Exactive quadrupole-Orbitrap hybrid high-resolution mass spectrometer with a heated-electrospray-ionization (HESI) source (Thermo Scientific, Waltham, MA, USA).

#### 4.6. Liquid Chromatography

Chromatographic separation occurred on a Kinetex<sup>®</sup> Biphenyl column (150  $\times$  2.1 mm, 2  $\mu\text{m}$ ) (Phenomenex, Castel Maggiore, Italy) maintained at  $37 \pm 1\text{ }^{\circ}\text{C}$ . The 30 min run utilized 0.1% formic acid in water (MPA) and 0.1% formic acid in acetonitrile (MPB) at a 0.4 mL/min flow rate. The gradient was started at 5% MPB for 2 min, increased to 25% MPB by 18 min, further increased to 95% MPB within 2 min, and held for 5 min. The return to initial conditions occurred within 0.1 min, followed by a 4.9 min equilibration, for a total runtime of 30 min. Autosampler temperature was  $10 \pm 1\text{ }^{\circ}\text{C}$ .



#### 4.7. Mass Spectrometry Conditions

Samples were injected twice, once in positive- and once in negative-ionization mode. HESI source parameters were 50 sheath-gas flow rate, 10 auxiliary-gas flow rate,  $\pm 3$  kV spray voltage, 300 °C capillary- and auxiliary-gas heater temperature, and 50 S-lens radio frequency; sweep gas was not applied. The orbitrap was calibrated prior to analysis, with a lock mass list for better accuracy. Data were acquired from 1 to 25 min in full-scan HRMS (FullMS)/data-dependent MS/MS (ddMS<sup>2</sup>) mode. The FullMS acquisition range was  $m/z$  120–700 with a resolution of 70,000 at full width at half maximum (FWHM) at  $m/z$  200. The automatic gain control (AGC) target was  $10^6$  and maximum injection time (IT) 200 ms. Up to 5 ddMS<sup>2</sup> scans were triggered, with a dynamic exclusion of 2.0 s and an intensity threshold of  $10^4$  for each FullMS scan, depending on a priority inclusion list of putative metabolites (Supplementary Table S1) based on *in silico* predictions and the metabolic fate of 4-AcO-DiPT analogues (Table 1). Other ions not in the inclusion list might also trigger ddMS<sup>2</sup> scans. Additionally, background  $m/z$  values with high intensity were assessed during injection of blank controls and compiled in an exclusion list in positive- and negative-ion modes. The ddMS<sup>2</sup> isolation window was  $m/z \pm 1.2$  with a resolution of 17,500 and the normalized collision energy (NCE) was 30, 60, and 90 a.u. The ddMS<sup>2</sup> AGC target was  $2 \times 10^5$  and maximum IT was 64 ms.

#### 4.8. Final Metabolite Identification

LC-HRMS data were processed with Compound Discoverer (v. 3.1.1.12) from Thermo Scientific (Waltham, MA, USA), using a partially automated approach. Briefly, the ions detected in HRMS were compared to a list of theoretical metabolites (intensity threshold,  $5 \times 10^3$ ; mass tolerance, 5 ppm). The HRMS/MS spectra and theoretical elemental composition of the ions were compared to online databases (intensity threshold,  $10^5$ ; HRMS mass tolerance, 5 ppm; HRMS/MS mass tolerance, 10 ppm). The chromatographic peaks detected in controls with a similar or higher intensity to that of the peaks detected in the samples were filtered out.

### 5. Conclusions

This study marks the first characterization of the 4-AcO-DiPT metabolic profile in human hepatocytes using *in silico* metabolite predictions, LC-HRMS/MS analysis, and software-assisted data mining. We identified six metabolites through ester hydrolysis followed by *N*-Deisopropylation, *O*-sulfation, *O*-glucuronidation, and/or *N*-Oxidation. We recommend 4-OH-DiPT, 4-OH-iPT, and 4-OH-DiPT-*N*-oxide as metabolite biomarkers of 4-AcO-DiPT consumption in clinical and forensic toxicology. We propose incorporation of HRMS/MS fragmentation patterns into the online libraries mzCloud and HighResNPS. These findings underscore the value of experimental data and demonstrate how challenging it is to predict NPS metabolism. Our *in vitro* model offers preliminary findings about 4-AcO-DiPT human metabolism; however, these findings should be verified using samples from authentic positive cases. These data enable analytical toxicologists to identify 4-AcO-DiPT exposure cases.

**Supplementary Materials:** The following supporting information can be downloaded at: <https://www.mdpi.com/article/10.3390/metabo12080705/s1>, Table S1: Inclusion list for the MS/MS data-dependent acquisition.

**Author Contributions:** Conceptualization, S.M., M.A.H. and J.C.; methodology, J.C.; formal analysis, S.M. and J.C.; data curation, S.M. and J.C.; writing—original draft preparation, S.M.; writing—review and editing, M.A.H., L.L., L.T.M., A.T., J.C. and F.P.B.; supervision, F.P.B.; project administration, J.C. and F.P.B.; funding acquisition, A.T. and F.P.B. All authors have read and agreed to the published version of the manuscript.

**Funding:** This research was funded by the Department for Antidrug Policies, in Italy, under the project “Effetti delle NPS: Sviluppo di una multicentrica di ricerca per il potenziamento informativo del Sistema di Allerta Precoce”.

**Institutional Review Board Statement:** Not applicable.

**Informed Consent Statement:** Not applicable.

**Data Availability Statement:** The data presented in this study are available in the main article and the supplementary materials.

**Acknowledgments:** The authors would like to thank Simonetta di Carlo, Antonella Bacosi, Michele Sciotti, and Laura Martucci for technical assistance.

**Conflicts of Interest:** The authors declare no conflict of interest.

## References

1. Rickli, A.; Moning, O.D.; Hoener, M.C.; Liechti, M.E. Receptor interaction profiles of novel psychoactive tryptamines compared with classic hallucinogens. *Eur. Neuropsychopharmacol.* **2016**, *26*, 1327–1337. [CrossRef]
2. Baumeister, D.; Barnes, G.; Giaroli, G.; Tracy, D. Classical hallucinogens as antidepressants? A review of pharmacodynamics and putative clinical roles. *Ther. Adv. Psychopharmacol.* **2014**, *4*, 156–169. [CrossRef]
3. Bunzow, J.R.; Sonders, M.S.; Arttamangkul, S.; Harrison, L.M.; Zhang, G.; Quigley, D.I.; Darland, T.; Suchland, K.L.; Pasumamula, S.; Kennedy, J.L.; et al. Amphetamine, 3,4-methylenedioxy methamphetamine, lysergic acid diethylamide, and metabolites of the catecholamine neurotransmitters are agonists of a rat trace amine receptor. *Mol. Pharm.* **2001**, *60*, 1181–1188. [CrossRef]
4. Cozzi, N.V.; Gopalakrishnan, A.; Anderson, L.L.; Feih, J.T.; Shulgin, A.T.; Daley, P.F.; Ruoho, A.E. Dimethyltryptamine and other hallucinogenic tryptamines exhibit substrate behavior at the serotonin uptake transporter and the vesicle monoamine transporter. *J. Neurotransm.* **2009**, *116*, 1591–1599. [CrossRef]
5. Fantegrossi, W.E.; Harrington, A.W.; Kiessel, C.L.; Eckler, J.R.; Rabin, R.A.; Winter, J.C.; Coop, A.; Rice, K.C.; Woods, J.H. Hallucinogen-like actions of 5-methoxy-*N,N*-diisopropyl-tryptamine in mice and rats. *Pharmacol. Biochem. Behav.* **2006**, *83*, 122–129. [CrossRef]
6. McKenna, D.J.; Repke, D.B.; Lo, L.; Peroutka, S.J. Differential interactions of indolealkylamines with 5-hydroxytryptamine receptor subtypes. *Neuropharmacology* **1990**, *29*, 193–198. [CrossRef]
7. Luethi, D.; Liechti, M.E. Monoamine transporter and receptor interaction profiles in vitro predict reported human doses of novel psychoactive stimulants and psychedelics. *Int. J. Neuropsychopharmacol.* **2018**, *21*, 926–931. [CrossRef] [PubMed]
8. Dos Santos, R.G.; Hallak, J.E.C. Therapeutic use of serotonergic hallucinogens: A review of the evidence and of the biological and psychological mechanisms. *Neurosci. Biobehav. Rev.* **2020**, *108*, 423–434. [CrossRef] [PubMed]
9. Acetoxy-DiPT Legal Status by Erowid. Available online: [https://erowid.org/chemicals/4\\_acetoxy\\_dipt/4\\_acetoxy\\_dipt\\_law.shtml](https://erowid.org/chemicals/4_acetoxy_dipt/4_acetoxy_dipt_law.shtml) (accessed on 9 June 2022).
10. Malaca, S.; Lo Faro, A.F.; Tamborra, A.; Pichini, S.; Busardò, F.P.; Huestis, M.A. Toxicology and Analysis of Psychoactive Tryptamines. *Int. J. Mol. Sci.* **2020**, *21*, 9279. [CrossRef] [PubMed]
11. Global Drug Survey (GDS). Available online: <https://www.globaldrugsurvey.com/wp-content/themes/globaldrugsurvey/results/GDS2019-Exec-Summary.pdf> (accessed on 9 June 2022).
12. 4-Acetoxy-DiPT Dosage by Erowid. Available online: [https://www.erowid.org/chemicals/4\\_acetoxy\\_dipt/4\\_acetoxy\\_dipt\\_dose.shtml](https://www.erowid.org/chemicals/4_acetoxy_dipt/4_acetoxy_dipt_dose.shtml) (accessed on 9 June 2022).
13. Zhang, Y.; Yuan, B.; Takagi, N.; Wang, H.; Zhou, Y.; Si, N.; Yang, J.; Wei, X.; Zhao, H.; Bian, B. Comparative Analysis of Hydrophilic Ingredients in Toad Skin and Toad Venom Using the UHPLC-HR-MS/MS and UPLC-QqQ-MS/MS Methods Together with the Anti-Inflammatory Evaluation of Indolealkylamines. *Molecules* **2018**, *24*, 86. [CrossRef] [PubMed]
14. Swortwood, M.J.; Carlier, J.; Ellefsen, K.N.; Wohlfarth, A.; Diao, X.; Concheiro-Guisan, M.; Kronstrand, R.; Huestis, M.A. In vitro, in vivo and in silico metabolic profiling of  $\alpha$ -pyrrolidinopentiothiophenone, a novel thiophene stimulant. *Bioanalysis* **2016**, *8*, 65–82. [CrossRef] [PubMed]
15. Diao, X.; Carlier, J.; Zhu, M.; Huestis, M.A. Human Hepatocyte Metabolism of Novel Synthetic Cannabinoids MN-18 and Its 5-Fluoro Analog 5F-MN-18. *Clin. Chem.* **2017**, *63*, 1753–1763. [CrossRef]
16. Caspar, A.T.; Gaab, J.B.; Michely, J.A.; Brandt, S.D.; Meyer, M.R.; Maurer, H.H. Metabolism of the tryptamine-derived new psychoactive substances 5-MeO-2-Me-DALT, 5-MeO-2-Me-ALCHT, and 5-MeO-2-Me-DIPT and their detectability in urine studied by GC-MS, LC-MSn, and LC-HR-MS/MS. *Drug Test. Anal.* **2018**, *10*, 184–195. [CrossRef] [PubMed]
17. Carlier, J.; Diao, X.; Huestis, M.A. Synthetic cannabinoid BB-22 (QUCHIC): Human hepatocytes metabolism with liquid chromatography-high resolution mass spectrometry detection. *J. Pharm. Biomed. Anal.* **2018**, *157*, 27–35. [CrossRef] [PubMed]
18. Diao, X.; Scheidweiler, K.B.; Wohlfarth, A.; Pang, S.; Kronstrand, R.; Huestis, M.A. In Vitro and In Vivo Human Metabolism of Synthetic Cannabinoids FDU-PB-22 and FUB-PB-22. *AAPS J.* **2016**, *18*, 455–464. [CrossRef]
19. Bruni, P.S.; Grafinger, K.E.; Nussbaumer, S.; König, S.; Schürch, S.; Weinmann, W. Study of the in vitro and in vivo metabolism of 4-HO-MET. *Forensic Sci. Int.* **2018**, *290*, 103–110. [CrossRef]
20. Grafinger, K.E.; Hädener, M.; König, S.; Weinmann, W. Study of the in vitro and in vivo metabolism of the tryptamine 5-MeO-MiPT using human liver microsomes and real case samples. *Drug Test. Anal.* **2018**, *10*, 562–574. [CrossRef]

21. Fabregat-Safont, D.; Barneo-Muñoz, M.; Martínez-García, F.; Sancho, J.V.; Hernández, F.; Ibáñez, M. Proposal of 5-methoxy-N-methyl-N-isopropyltryptamine consumption biomarkers through identification of in vivo metabolites from mice. *J. Chromatogr. A* **2017**, *1508*, 95–105. [[CrossRef](#)]
22. Manier, S.K.; Felske, C.; Zapp, J.; Eckstein, N.; Meyer, M.R. Studies on the In Vitro and In Vivo Metabolic Fate of the New Psychoactive Substance N-Ethyl-N-Propyltryptamine for Analytical Purposes. *J. Anal. Toxicol.* **2021**, *45*, 195–202. [[CrossRef](#)]
23. Michely, J.A.; Helfer, A.G.; Brandt, S.D.; Meyer, M.R.; Maurer, H.H. Metabolism of the new psychoactive substances N,N-diallyltryptamine (DALT) and 5-methoxy-DALT and their detectability in urine by GC-MS, LC-MSn, and LC-HR-MS-MS. *Anal. Bioanal. Chem.* **2015**, *407*, 7831–7842. [[CrossRef](#)]
24. Kamata, T.; Katagi, M.; Kamata, H.T.; Miki, A.; Shima, N.; Zaitso, K.; Nishikawa, M.; Tanaka, E.; Honda, K.; Tsuchihashi, H. Metabolism of the psychotomimetic tryptamine derivative 5-methoxy-N,N-diisopropyltryptamine in humans: Identification and quantification of its urinary metabolites. *Drug Metab. Dispos.* **2006**, *34*, 281–287. [[CrossRef](#)] [[PubMed](#)]
25. Kops, C.B.; Šícho, M.; Mazzolari, A.; Kirchmair, J. GLORYx: Prediction of the Metabolites Resulting from Phase 1 and Phase 2 Biotransformations of Xenobiotics. *Chem. Res. Toxicol.* **2021**, *34*, 286–299. [[CrossRef](#)] [[PubMed](#)]
26. Stork, C.; Embruch, G.; Šícho, M.; Kops, C.B.; Chen, Y.; Svozil, D.; Kirchmair, J. NERDD: A web portal providing access to in silico tools for drug discovery. *Bioinformatics* **2020**, *36*, 1291–1292. [[CrossRef](#)] [[PubMed](#)]
27. Di Trana, A.; Brunetti, P.; Giorgetti, R.; Marinelli, E.; Zaami, S.; Busardò, F.P.; Carlier, J. In silico prediction, LC-HRMS/MS analysis, and targeted/untargeted data-mining workflow for the profiling of phenylfentanyl in vitro metabolites. *Talanta* **2021**, *235*, 122740. [[CrossRef](#)] [[PubMed](#)]